

## Solar activity variations of equivalent winds derived from global ionosonde data

Libo Liu,<sup>1</sup> Xiaoli Luan,<sup>2,3</sup> Weixing Wan,<sup>1</sup> Jiuhou Lei,<sup>2,3</sup> and Baiqi Ning<sup>1</sup>

Received 5 May 2004; revised 15 September 2004; accepted 27 September 2004; published 15 December 2004.

[1] The equivalent winds at the  $F$  layer peak are derived from global ionosonde data to investigate their solar activity variations. With increasing solar activity, the derived equivalent winds are found of nonlinearly decreased diurnal amplitudes in all seasons at most stations. This implies that the increase in ion drag more than compensates for pressure gradients and thus restrains the diurnal amplitude at high solar activity. The diurnal phase of the derived equivalent winds generally shifts later at higher solar activity. It is the first time to explicitly report this striking feature that emerged at so many stations. Another pronounced feature is that the diurnal phase has a summer-winter difference. The diurnal phases at most stations in the Northern Hemisphere are later in winter than in summer at higher solar activity. Furthermore, a decrease in the semidiurnal amplitudes of equivalent winds with increasing solar activity is evident in winter over most stations considered and in other seasons at stations with a lower dip, but the decrease trend becomes weak in other seasons at stations with a larger dip. However, complicated dependences on solar activity can be found in the diurnal mean and the semidiurnal phases of equivalent winds at stations considered. **INDEX TERMS:** 2427 Ionosphere: Ionosphere/atmosphere interactions (0335); 3369 Meteorology and Atmospheric Dynamics: Thermospheric dynamics (0358); 3309 Meteorology and Atmospheric Dynamics: Climatology (1620); 2162 Interplanetary Physics: Solar cycle variations (7536); **KEYWORDS:** ionosphere, climatology, solar activity variation

**Citation:** Liu, L., X. Luan, W. Wan, J. Lei, and B. Ning (2004), Solar activity variations of equivalent winds derived from global ionosonde data, *J. Geophys. Res.*, 109, A12305, doi:10.1029/2004JA010574.

### 1. Introduction

[2] Understanding the variations of thermospheric winds is an important subject involving the upper atmosphere and the ionosphere. During the past decades, many efforts have been directed to investigate the seasonal and solar activity variations of the thermospheric neutral winds, and results are continuously being updated by many means with the development of techniques and the increase of multiple data sets in hand [e.g., Buonsanto, 1990, 1991; Biondi *et al.*, 1991, 1999; Duboin and Lafeuille, 1992; Hagan, 1993; Arriagada *et al.*, 1997; Buonsanto and Witasse, 1999; Igi *et al.*, 1999; Kawamura *et al.*, 2000; Foppiano *et al.*, 2003].

[3] Up to now, patterns of the solar activity trends in neutral winds are still confused. Significant differences were found in the solar activity dependences of the diurnal mean and diurnal amplitude of winds from various data sets and models. With increasing solar activity, the diurnal amplitude of the meridional wind was found to decrease at some locations, but the opposite trend was also found in some seasons and at some

locations [e.g., Buonsanto, 1991; Duboin and Lafeuille, 1992; Aruliah *et al.*, 1996; Arriagada *et al.*, 1997]. A decrease in the diurnal amplitude was found at some midlatitude stations [Buonsanto, 1991; Hedin *et al.*, 1994]. Similar trends were reported in the diurnal ionosonde winds at a low-latitude station, Wuhan (114.4°E, 30.6°N) [Liu *et al.*, 2003c]. In contrast, a higher solar flux results in a larger meridional wind at Kiruna (67.8°N, 20.4°E) of Sweden for each season [Aruliah *et al.*, 1996]. Furthermore, at a southern midlatitude station, King George Island (62.2°S, 58.8°W), the wind amplitudes decrease from low to high solar activity levels in spring and summer but increase in winter [Arriagada *et al.*, 1997]. Similarly, the solar cycle variations of the diurnal mean wind are also complicated [e.g., Hedin *et al.*, 1994; Igi *et al.*, 1999; Liu *et al.*, 2003c]. Therefore the details of the solar activity trends may differ from study to study and from location to location. In addition, the phases of the tidal components of winds attract much less attention.

[4] This paper investigates the equivalent winds deduced from monthly median ionosonde data at global 39 stations from June 1954 to February 2004. The aim of the present work is to identify the solar activity dependences of the diurnal mean and dominant tidal components of the derived equivalent winds.

### 2. Data and Analysis Method

[5] Equivalent winds in the magnetic meridian can be deduced from ionosonde measurements [Titheridge,

<sup>1</sup>Institute of Geology and Geophysics, Chinese Academy of Sciences, Beijing, China.

<sup>2</sup>Wuhan Institute of Physics and Mathematics, Chinese Academy of Sciences, Wuhan, China.

<sup>3</sup>Also at Graduate School of Chinese Academy of Sciences, Beijing, China.

**Table 1.** List of the Ionosonde Stations From Which Ionospheric Data Were Selected

Station	Geographic		Geomagnetic Latitude	Dip	Declination	Years Analyzed
	Latitude	Longitude				
Yakutsk	62.0	129.6	51.3	75.7	-12.2	1957–1991
Tomsk	56.5	84.9	46.1	74.0	7.1	1957–2002
Novosibirsk	54.6	83.2	44.3	72.5	6.8	1969–2002
Sverdlovsk	56.4	58.6	48.5	72.2	10.5	1957–1995
Magadan	60.0	151.0	51.0	71.2	-8.5	1968–2002
Gorky	56.1	44.3	50.3	71.2	8.4	1958–1989
Irkutsk	52.5	104.0	41.3	71.0	-2.2	1958–1996
Moscow	55.5	37.3	50.7	70.4	6.5	1957–2002
Kaliningrad	54.7	20.6	52.9	69.1	1.3	1964–1994
Karaganda	49.8	73.1	40.4	68.2	6.7	1964–1989
Wallops Is.	37.9	284.5	49.0	68.1	-9.2	1967–2004
Boulder	40.0	254.7	48.9	67.7	11.6	1958–2002
Kiev	50.5	30.5	47.1	66.5	3.8	1964–1992
Petropavlovsk	53.0	158.7	45.0	64.6	-4.3	1968–2002
Rostov	47.2	39.7	42.4	64.2	4.9	1958–2002
Lannion	48.5	356.7	51.6	64.0	-7.3	1971–1989
Novokazalinsk	45.5	62.0	37.4	63.9	5.6	1964–1989
Khabarovsk	48.5	135.1	38.2	63.6	-9.5	1959–1993
Poitiers	46.6	0.3	49.1	62.3	-5.5	1964–1989
Alma Ata	43.3	76.9	33.5	62.1	3.7	1957–1989
Tashkent	41.3	69.6	32.4	59.9	3.7	1961–1996
Point Arguello	34.6	239.4	41.3	59.8	14.5	1971–2004
Wakkanai	45.4	141.7	35.7	59.4	-8.0	1949–2003
Tbilisi	41.7	44.8	36.2	59.4	4.2	1963–1986
Sofia	42.7	23.4	40.9	59.1	1.4	1988–2003
Ashkhabad	37.9	58.3	30.4	55.8	3.3	1957–1995
Akita	39.7	140.1	29.9	53.5	-6.5	1968–1988
El Arenosillo	37.1	353.3	41.3	52.2	-7.1	1982–1999
Kokubunji	35.7	139.5	25.9	48.8	-5.4	1957–2003
Yamagawa	31.2	130.6	20.7	43.9	-4.5	1965–2003
Maui	20.8	203.5	21.2	38.5	11.3	1957–1994
Okinawa	26.3	127.8	15.6	36.5	-3.2	1957–2003
Townsville	-19.3	146.7	-28.0	-49.1	7.5	1963–2002
Port Stanley	-51.7	302.2	-40.7	-49.2	4.8	1967–2004
Brisbane	-27.5	152.9	-35.3	-58.1	10.7	1957–1986
Grahamstown	-33.3	26.5	-34.0	-64.2	-22.6	1973–2004
Canberra	-35.3	149.0	-43.5	-66.4	11.7	1954–2004
Mundaring	-32.0	116.3	-43.1	-66.7	-3.1	1960–2004
Hobart	-42.9	147.2	-51.3	-73.0	13.7	1954–2004

1995], and many derivation techniques have been developed [e.g., Miller *et al.*, 1986, 1997; Buonsanto, 1990; Titheridge, 1995; Liu *et al.*, 2003b]. Those derivation techniques rely on the strong coupling between the  $F$  region ionization and the neutral winds or  $\mathbf{E} \times \mathbf{B}$  drifts. The equivalent winds generally refer to the combined contribution on the ionospheric plasma movement from the horizontal neutral meridional winds and the north perpendicular  $\mathbf{E} \times \mathbf{B}$  drifts. We call the projection of the contributions from the  $\mathbf{E} \times \mathbf{B}$  drifts and the meridional winds in the vertical direction as vertical equivalent winds (VEWs) in this work. The contributions from the  $\mathbf{E} \times \mathbf{B}$  drifts should be subtracted to give the true neutral winds. Fortunately, its effect is insignificant [Miller *et al.*, 1987] for the mean and quiet conditions at midlatitudes, even for locations with a magnetic latitude as low as  $19.7^\circ\text{N}$  at Wuhan [Liu *et al.*, 2003b]. Therefore to avoid introducing possible false information from an estimated  $\mathbf{E} \times \mathbf{B}$  drift, corrections for drifts due to electric fields are not included in this work. Further, the possible effects induced by the vertical thermospheric winds are also ignored. In other words, the vertical neutral winds were assumed to be zero.

[6] The method used in this paper for deriving equivalent winds from the critical frequency ( $f_oF2$ ) and peak height ( $hmF2$ ) of the  $F$  layer has been described by Luan *et al.* [2002] and Liu *et al.* [2003b] in detail. It has been applied to investigate the seasonal and solar activity variations of equivalent winds over Wuhan [Liu *et al.*, 2003a, 2003c].

[7] The database used in the present work, available from the U.S. National Geophysical Data Center (NGDC-NOAA) database and the World Data Center (WDC), Tokyo for Ionosphere, consists of the monthly median values of  $f_oF2$ ,  $M3000F2$ , and  $f_oE$  from the ionosonde stations, as listed in Table 1.  $M3000F2$  is the ratio of  $MUF(3000)F2$ , the  $F2$  layer 3000 km maximum usable frequency, to  $f_oF2$ , while  $f_oE$  is the critical frequency of the  $E$  layer. The values of  $hmF2$  are estimated from the monthly median  $f_oF2$ ,  $M3000F2$ , and  $f_oE$  with the well-known statistical relationship [Dudeney, 1983].

[8] To obtain detailed information on the solar activity trends, data will be shown over the full range of solar activity in season, not sorted into two solar activity levels (solar minimum and maximum). This differs from most previous studies. Thus simultaneous observations of

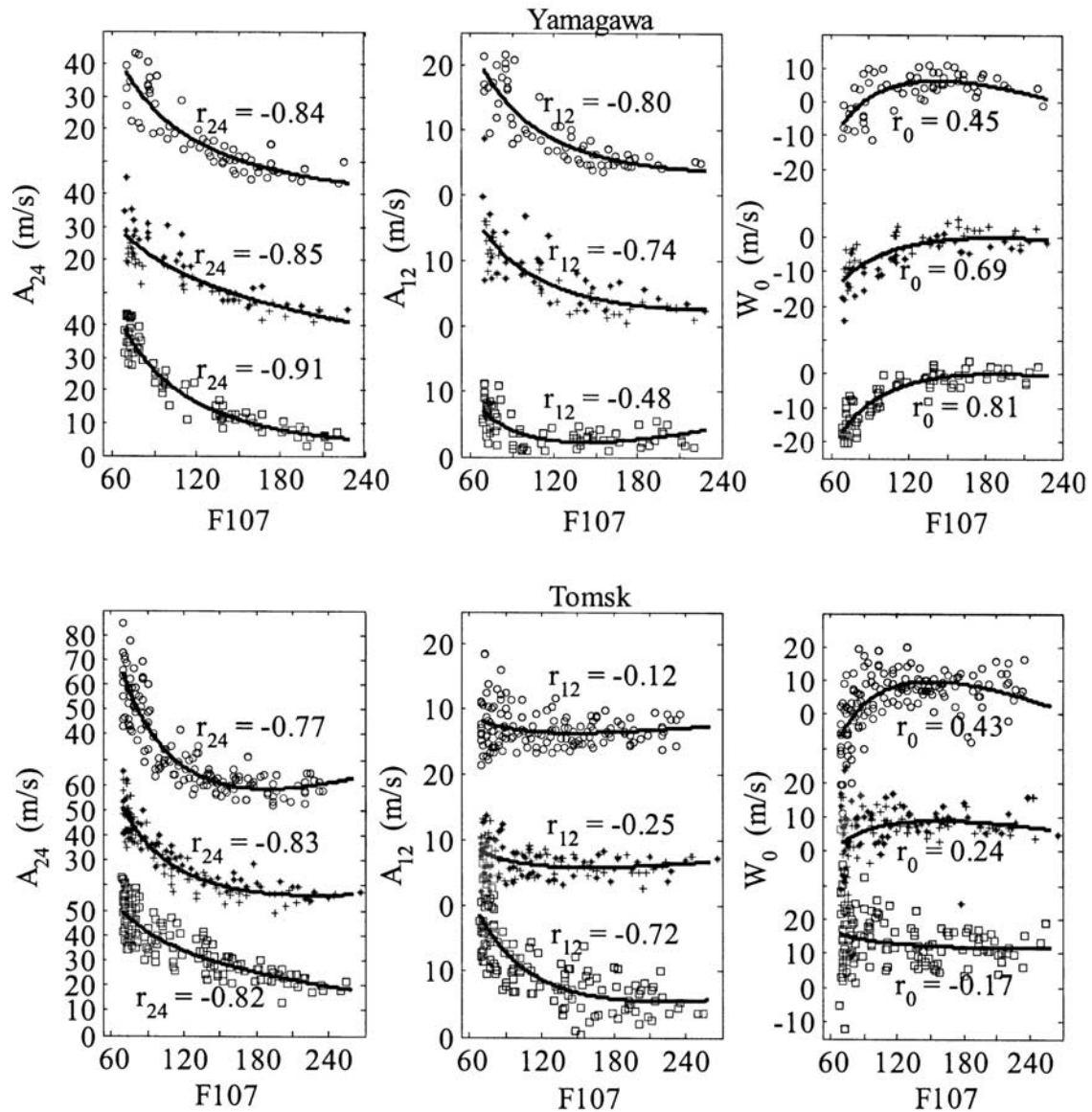


**Figure 1.** The diurnal ( $A_{24}$ ) and semidiurnal ( $A_{12}$ ) amplitudes and the diurnal mean ( $W_0$ ) winds versus solar activity  $F107$  at Yamagawa ( $31.2^\circ\text{N}$ ,  $130.6^\circ\text{E}$ ) and Tomsk ( $56.5^\circ\text{N}$ ,  $84.9^\circ\text{E}$ ). Points with plus, open-circle, asteroid, and square symbols represent for seasons from spring equinox months, summer, autumn months, and winter, respectively. The lines show the least squares fit trends. The  $r_{24}$ ,  $r_{12}$ ,  $r_0$  represent for the corresponding correlation coefficients of the diurnal, semidiurnal, and the diurnal mean winds with  $F107$ , respectively. The spring equinox and autumn months are combined as equinox.

monthly median  $foF_2$ ,  $M3000F_2$ , and  $foE$  should cover more than a full solar activity. To eliminate the influence of very high geomagnetic activities, we use median values and reject those months with monthly mean  $A_p$  index higher than 20. Months from November to February are sorted as winter, March and April are sorted as spring, May to August are sorted as summer, and September and October are sorted as fall in the Northern Hemisphere. Although there may exist an equinox asymmetry [e.g., Aruliah et al., 1996; Liu et al., 2003a], the data in spring and fall were also sorted as equinoxes to provide enough data for statistical analysis. Ionosonde measurements at 39 stations (Table 1) are adopted. Most stations are located at magnetic

latitudes between  $30^\circ$  and  $50^\circ$  in the European and Asian sectors ( $330\sim 160^\circ\text{E}$ ). Only several southern stations have sufficient data for the study requirement.

[9] A least-squares analysis is performed on the derived equivalent winds for each month using the following equation [e.g., Duboin and Lafeuille, 1992]:

$$VEW(t) = W_0 + A_{24} \cos[\omega_{24}(t - t_{24})] + A_{12} \cos[\omega_{12}(t - t_{12})] + A_8 \cos[\omega_8(t - t_8)] + I(e), \quad (1)$$

where  $VEW$  is the projection of equivalent winds in the vertical direction,  $W_0$  is the diurnal mean of  $VEW$ ,  $A_n$  and  $t_n$

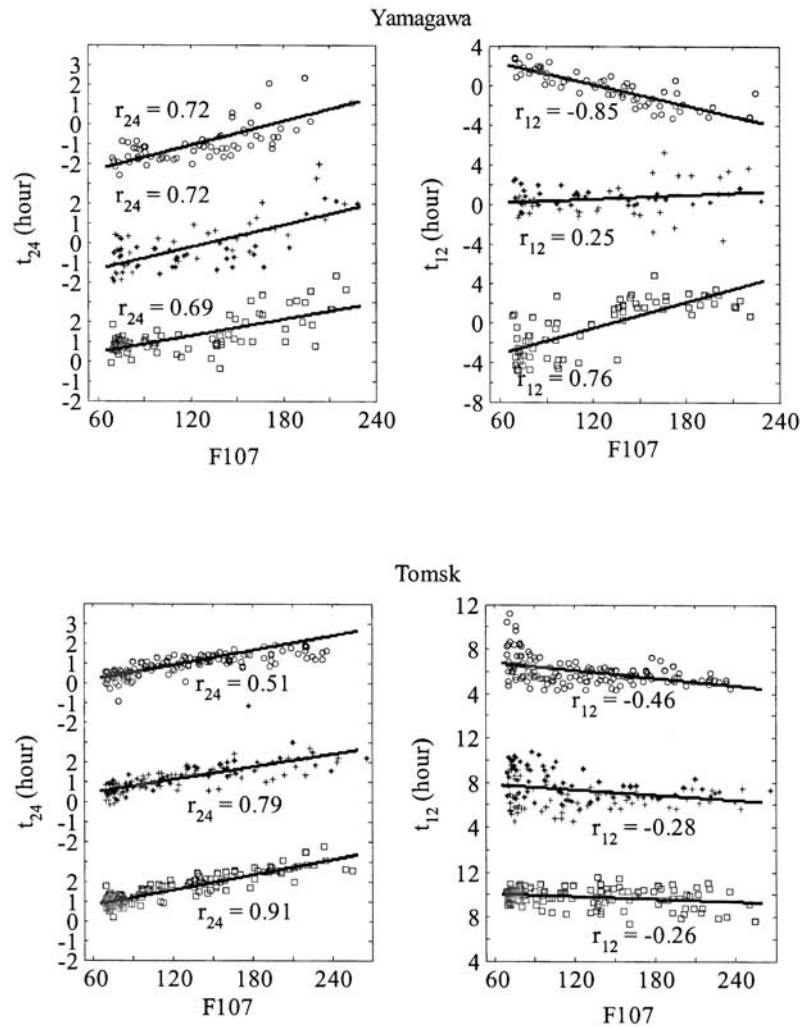


**Figure 2.** Same as Figure 1, but for the diurnal ( $t_{24}$ ) and semidiurnal ( $t_{12}$ ) phases at the two stations.

are the amplitudes and phases of the tidal components, respectively, and the angular frequency  $\omega_n = 2\pi/n$ ,  $n = 24, 12, 8$ . Here  $t$  is the local time in hours and  $l(e)$  is the corresponding error term. In this work,  $t_n$  represents the local time when the corresponding tidal component reaches its upward maximum (or the equatorward maximum for the meridional winds).

### 3. Results

#### 3.1. Sample Stations

[10] The amplitudes and phases of the tidal components decomposed from the VEWs at Yamagawa (31.2°N, 130.6°E, dip 43.9°) and Tomsk (56.5°N, 84.9°E, dip 74°) are presented in Figures 1–2 as examples. The diurnal component predominates in the VEWs at both stations. As shown in Figures 1 and 2, at both stations, the diurnal amplitudes and phases of the VEWs reveal a clear solar activity trend in all seasons. With increasing  $F107$ , the diurnal amplitude nonlinearly decreases at both stations, and the diurnal phase obviously tends to shift later.

[11] Similar to the diurnal amplitude ( $A_{24}$ ), the semidiurnal amplitude ( $A_{12}$ ) at Yamagawa also has a significantly negative solar activity trend in summer and equinoxes and a

weaker one in winter. In contrast, at Tomsk, the semidiurnal amplitude generally has a fairly weak solar activity variation except in winter when it has an obvious decrease trend. The semidiurnal phase ( $t_{12}$ ) generally distributes scattered compared with the diurnal one (Figure 2), and its solar activity trends differ at the two stations. At Tomsk, the semidiurnal phase has a weak correlation with  $F107$  for all seasons, whereas at Yamagawa, it has strong a negative correlation with  $F107$  in summer, weak in equinox, and strongly positive in winter.

[12] At Yamagawa, the diurnal mean equivalent winds significantly decrease from downward flows to zero in equinoxes and winter and are relatively poorly correlated with  $F107$  in summer, while at Tomsk, the solar activity trends of the diurnal mean winds are weak in equinoxes and winter and relatively clear in summer.

[13] The solar activity trends of tidal winds, which are represented by their correlation with  $F107$ , are labeled particularly at Maui (20.8°N, 203.5°E, dip 38.5°), Grahams-town (33.3°S, 26.5°E, dip -64.2°), Boulder (40.0°N, 254.7°E, dip 67.7°), Kokubunji (35.7°N, 139.5°E, dip 48.8°), and Port Stanley (51.7°S, 302.2°E, dip -49.2°) with symbols M, G, B, K, and PS in Figure 3 and other figures, respectively. The equivalent winds at the later three stations

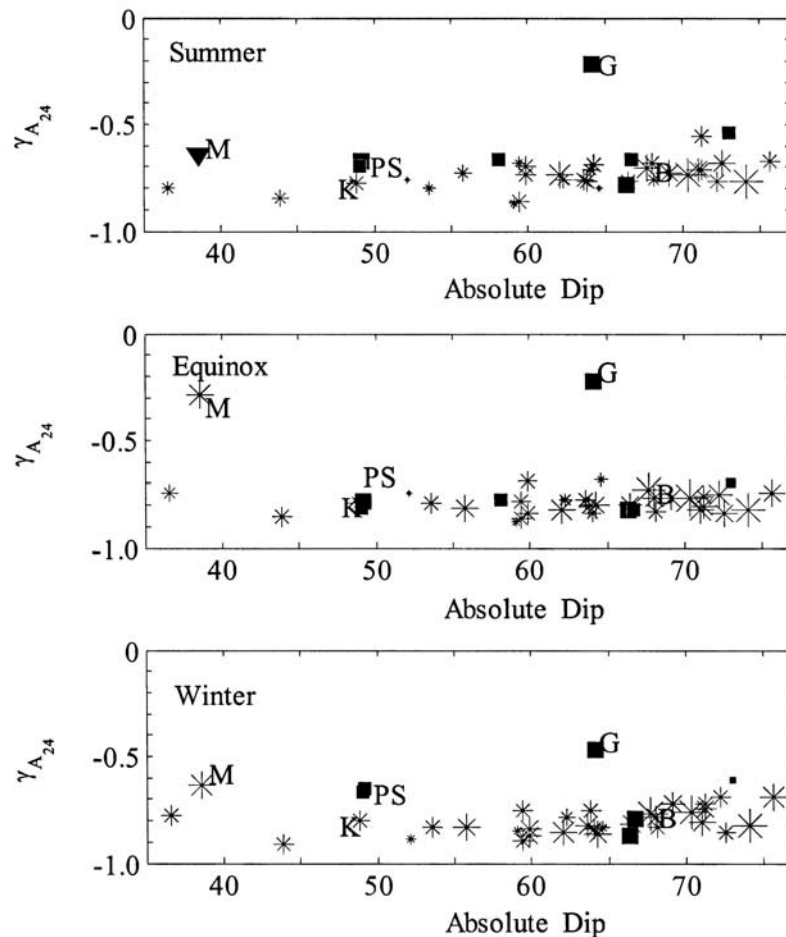


**Figure 3.** The correlation coefficients ( $\gamma_{A_{24}}$ ) of the diurnal amplitudes with  $F_{107}$  for summer, equinoxes, and winter months at stations listed in Table 1. Points with asterisk and square symbols represent the values for the Northern and Southern Hemisphere stations, respectively. The unique triangle in the top panel represents for  $-\gamma_{A_{24}}$  in summer at Maui. The size of the symbols illustrates the number of valid data at each station with the least  $\sim 20$ – $33$ . The results at Maui (M), Grahamstown (G), Kokubunji (K), Boulder (B), and Port Stanley (PS) are labeled particularly.

have been investigated by *Buonsanto* [1991], *Igi et al.* [1999], and *Foppiano et al.* [2003], respectively. As seen in Figure 3, our results for those stations are generally consistent with past investigations.

### 3.2. Diurnal Amplitudes and Phases

[14] The nonlinear solar activity dependences of the diurnal component at most stations are generally similar to those at Yamagawa and Tomsk. Figure 3 shows the correlations between  $F_{107}$  and the diurnal amplitude of the VEWs at 39 stations considered. There are generally strong inverse solar activity dependences in the diurnal amplitude in all seasons and at all stations except Grahamstown and Maui. At Grahamstown, the trends are a little weaker in winter and not obvious in summer and equinoxes, while at Maui, the trends are weak in equinox and positive in summer (its correlation coefficient  $\gamma_{A_{24}}$  higher than 0.6), which is unique and distinctly different from other stations considered. At most stations, the absolute values of  $\gamma_{A_{24}}$  are mostly higher than 0.7 for all seasons.

[15] The diurnal phase ( $t_{24}$ ) represents the local time when the diurnal component of the VEWs reaches its

upward maximum (or the equatorward maximum for the meridional winds). The correlations between  $F_{107}$  and the diurnal phase at the stations considered are generally strong, as shown in Figure 4. The values of  $\gamma_{t_{24}}$  are also generally higher than 0.7, which reveals that the solar activity trends in the diurnal phase are very similar at most stations considered, and  $t_{24}$  tends to shift later from local late evening to early morning with increasing solar activity. However, it has not attracted enough attention in previous investigations, and this common and evident feature is reported explicitly for the first time. Relatively weaker, or not obvious solar activity trends of the diurnal phases are found in summer and equinox at some stations, including Maui, Grahamstown, Townsville ( $19.3^{\circ}\text{S}$ ,  $146.7^{\circ}\text{E}$ , dip  $-49.1^{\circ}$ ), and Wallops Island ( $37.9^{\circ}\text{N}$ ,  $284.5^{\circ}\text{E}$ , dip  $68.1^{\circ}$ ).

[16] Besides the solar activity variation, the winds are strongly dependent on season. The diurnal phase was reported to be the latest in winter and at solar maximum for the ionosonde winds at Boulder and three southern midlatitude stations [*Buonsanto*, 1991; *Foppiano et al.*, 2003]. To illustrate the seasonal behavior,  $t_{24}$  in summer

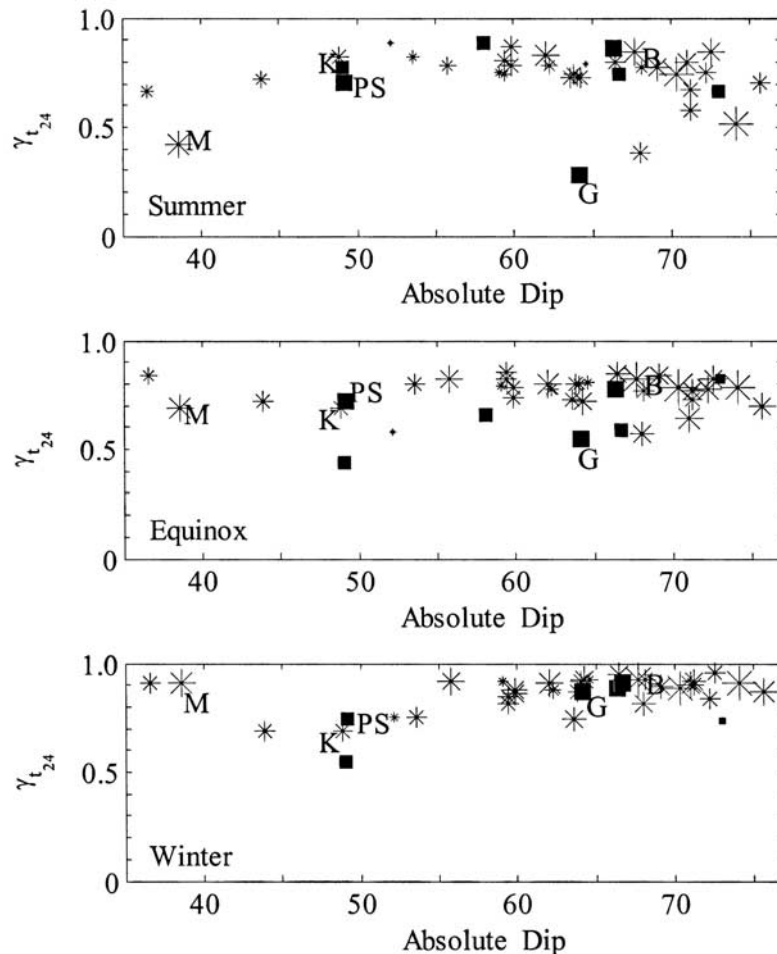


**Figure 4.** Same as Figure 3, but for the diurnal phase  $t_{24}$ .

and winter at seven northern stations and three southern stations are shown in Figure 5.

[17] There are seasonal dependences in the solar activity trends of the diurnal phase (Figures 2 and 5). At these stations, the diurnal component reaches its upward maximum mostly at 0000 ~ 0400 LT in winter and 2300 ~ 0200 LT in summer from low to high solar activity, except that it shifts by ~4 hours at Maui in both seasons. Generally, the diurnal phase is later in winter than in summer from moderate to high solar activity in the Northern Hemisphere. In contrast, at the three southern stations the seasonal variations of the diurnal phase are complicated. From low to high solar activity, it tends to be later in summer at Port Stanley, opposite at Canberra (35.3°S, 149.1°E, dip  $-66.4^\circ$ ), and a shift from later to earlier at Grahamstown. The behaviors at Port Stanley are opposite to the general trends at the northern stations. In addition, the diurnal phase is much closer to each other in summer and winter at solar maximum at Canberra and Wakkanai, which differs from most other stations.

### 3.3. Semidiurnal Amplitudes and Phases

[18] Figures 6 and 7 respectively illustrate the correlations between  $F107$  and the semidiurnal amplitudes ( $A_{12}$ ) and phases ( $t_{12}$ ) of the VEWs at stations considered as a function of the absolute dip angle. Compared with the diurnal component, the solar activity dependences of the

semidiurnal components are complicated and relatively insignificant at most stations.

[19] There is a solar activity dependence of  $A_{12}$  on the dip angle. With the absolute dip angle increasing from  $\sim 35^\circ$  to  $76^\circ$ , the solar cycle trends of  $A_{12}$  shift from strong decrease to fairly weak in summer and equinox, and even turn to be weak increase except at Grahamstown, where the trend is a marked increase in equinox. In winter, the trends are significant at most stations, although fairly weak at several stations including Boulder.

[20] The trends of the semidiurnal phase  $t_{12}$  with  $F107$  are complicated and inconsistent from station to station. Their dip angle dependences are more obvious in summer and weak in equinox and winter. In winter, the correlation between  $t_{12}$  and  $F107$ , whether positive or not, is mostly strong at lower dip angles and turns weak at stations with a larger dip. The coefficients of the correlation between  $t_{12}$  and  $F107$  are distinctly different between Maui and other low latitude stations in equinox and winter.

### 3.4. Diurnal Mean

[21] As shown in Figure 1, the diurnal mean winds have seasonal and solar activity variations. The diurnal mean equivalent winds tend to decrease to a smaller flow with increasing solar activity. However, their detail solar activity dependences are related with the absolute values and directions of winds. The coefficients of the correlation

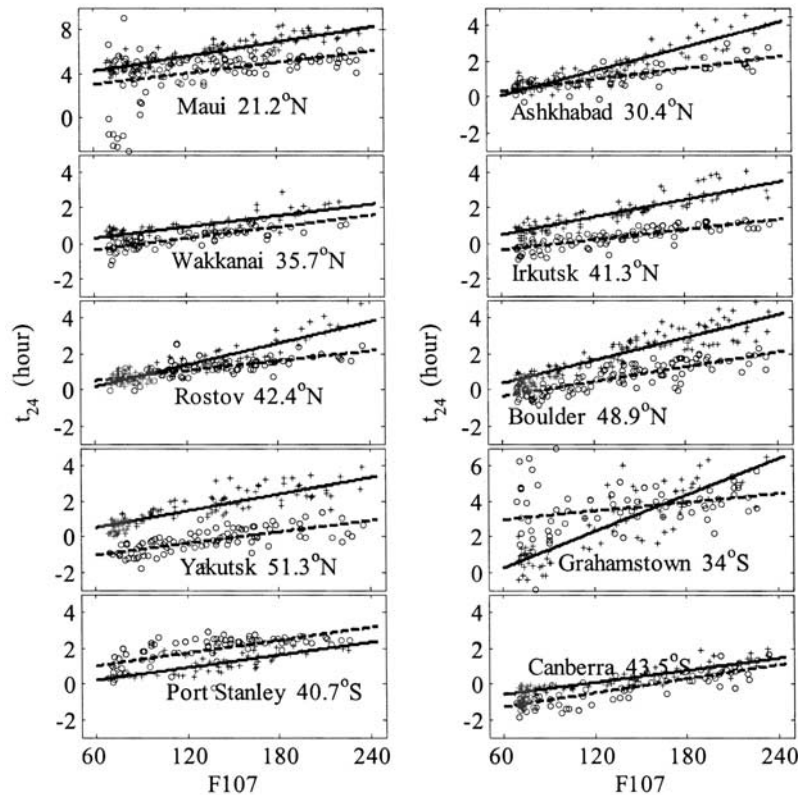


**Figure 5.** The diurnal phases  $t_{24}$  versus solar activity in summer (circles) and winter (pluses) at ten stations. Solid and dashed lines illustrate the least squares fit trends in summer and winter, respectively. The magnetic latitudes of stations are also labeled in the panels.

between the diurnal mean VEWs and  $F107$  are shown in Figure 8.

[22] Similar to the semidiurnal phase, the diurnal mean winds have complicated solar activity dependences. The solar activity trends of the diurnal mean winds are also somewhat dependent on the dip angle. With increase dip angle, the solar activity trends in the diurnal mean VEWs become positive to weak negative in winter and equinox and more irregular in summer.

## 4. Discussions

### 4.1. Effect of Ion Drag

[23] At low-latitude and midlatitude  $F$  region, the winds are primarily driven by pressure gradients generated by the solar radiations during daytime and auroral heating (in aurora regions) and retarded mainly by ion drags. With increasing solar activity, the pressure gradients and ion drags are expected to enhance with increase in atmospheric temperature and overall density. Although each is of solar activity dependent, their effects appear to cancel each other out. As previous works have pointed out, the balance between them will determine the winds with little or significant solar activity trend [e.g., Hedin *et al.*, 1994; Titheridge, 1995]. On the other hand, investigations on the solar activity trend in the thermospheric winds will improve the understanding of the balance between pressure gradients and ion drags.

[24] Examination of Figure 3 shows the decrease trends in the diurnal amplitudes with increasing  $F107$  at most

stations for all seasons, which verify the suggestion of Hedin *et al.* [1994] that this signature is not a feature of a particular location and also implies that the larger ion drag must play a more important role in restraining the amplitude at high solar activity as previously suggested [Hagan and Oliver, 1985; Buonsanto and Witasse, 1999; Kawamura *et al.*, 2000; Liu *et al.*, 2003c]. Similarly, Hedin *et al.* [1994] and Richards [2001] reported a decrease trend in equivalent wind at noon and at midnight as solar activity increases. Similar trends have also been found at Wuhan [Liu *et al.*, 2003c]. In addition, for most stations considered, the correlations of both the diurnal amplitude and phase with  $F107$  are a little stronger in winter than in summer (Figures 3 and 4), which is also in good agreement with the larger ion drag coefficient in winter than in summer at solar maximum [Forbes and Garrett, 1978].

[25] As described in section 3, the diurnal phase in Figures 4 and 5 tends to shift from local late evening to early morning with increasing solar activity, and this trend is almost identical at most stations considered. This striking feature that emerged at so many stations is reported explicitly for the first time.

[26] The solar activity and seasonal dependences of the diurnal phase are generally consistent with those at Boulder [Buonsanto, 1991] and Kokubunji [Igi *et al.*, 1999] for a full solar activity. However, it is contradicted with the ones derived from the ISR winds over Saint Santin ( $47.4^{\circ}\text{N}$ ,  $2.3^{\circ}\text{E}$ ) [Duboin and Lafeuille, 1992], Millstone Hill ( $43^{\circ}\text{N}$ ,  $72^{\circ}\text{W}$ ) [Hagan, 1993; Buonsanto

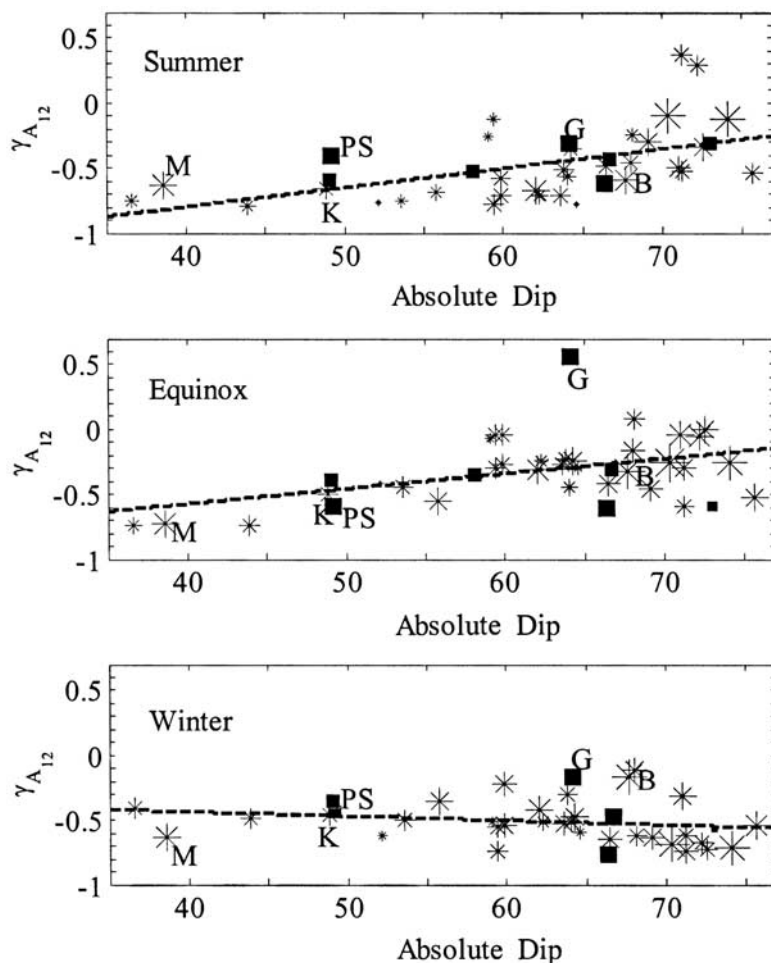


**Figure 6.** The correlation coefficients ( $\gamma_{A_{12}}$ ) of the semidiurnal amplitudes  $A_{12}$  with F107 for summer, equinoxes, and winter months at stations listed in Table 1. Points with asteroid and square symbols represent the values for the Northern and Southern Hemisphere stations, respectively. The size of the symbols illustrates the number of valid data at each station with the least  $\sim 35$ –44. The results at Maui (M), Grahamstown (G), Kokubunji (K), Boulder (B), and Port Stanley (PS) are labeled particularly.

and Witasse, 1999], and Shigaraki [Kawamura *et al.*, 2000]. The diurnal phase of the ISR winds appeared nearly stable under different solar activity levels and has no apparent seasonal variations. Therefore there are significant differences between the trends of the diurnal phase in the ISR winds and the ionosonde winds, which also need further investigation.

[27] The peak height of the  $F_2$  layer height varies with local time and solar activity. Generally speaking, it is higher at night and lower during sunrise periods at middle latitudes. And the peak height tends to increase with the increase of the solar activity at all local times. One limitation of the ionosonde winds is the equivalent winds can only be derived at the  $F$  layer peak, which is varied with local time and solar activity. Conversely, the ISR winds are generally evaluated at a constant height. This makes it difficult to compare the ionosonde winds with other techniques. Phase variations and large wind gradients are found at heights even up to 350 km from the EISCAT ISR wind profiles [Witasse *et al.*, 1998]; thus height gradient of the winds may have some effects on the results of the equivalent winds. On the other hand, owing to very

high viscosity at altitudes around the  $F_2$  layer peak height, small height gradients of the winds can be expected near the  $F$  layer peak.

[28] To access the competing balance between the driving force and the ion drag, we calculated the horizontal pressure gradient ( $F_H$ ) and the neutral-ion collision frequency ( $\nu_{ni}$ ) using the empirical IR100 [Bilitza, 2001] and MSISE00 models [Picone *et al.*, 2002] with observed  $hmF2$  and  $foF2$  for the input parameters. Ignoring the inertial term, viscosity, and the Coriolis force, the ratio of  $F_H$  and  $m_O\nu_{ni}$  can simply be taken as an indicator of equivalent winds [Buonsanto and Witasse, 1999]. Here  $m_O$  is the mass of atom O.

[29] Figure 9 shows the monthly median NmF2, VEWs, the horizontal pressure gradient force  $F_H$ , and the neutral-ion collision frequency  $\nu_{ni}$ , and their corresponding median values at Boulder in December for solar maximum ( $F107 > 180$ ), and solar minimum ( $F107 < 90$ ). The ratio,  $F_H/m_O\nu_{ni}$ , and its diurnal component are also illustrated in Figure 9. With increasing solar activity, the magnitude of the pressure gradient  $F_H$  is enhanced at most hours, especially larger during daytime, and so is the neutral-ion collision

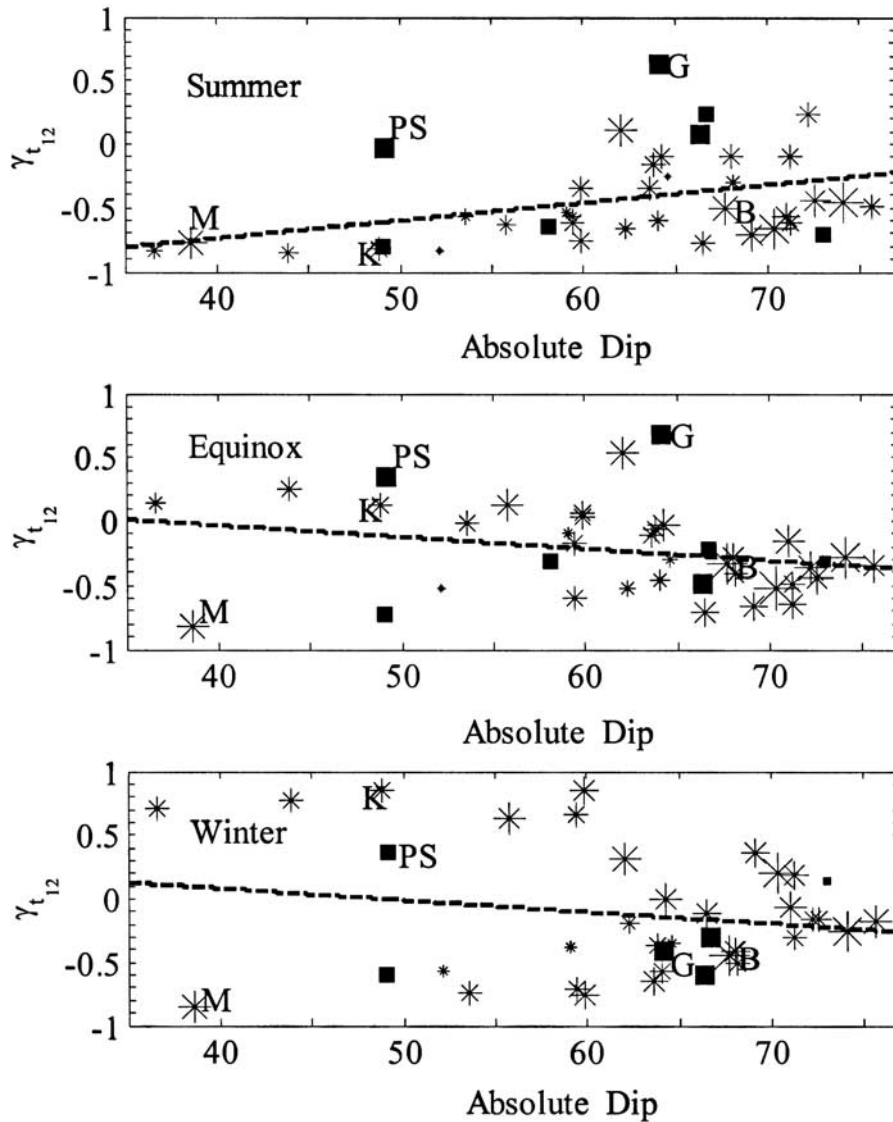


Figure 7. Same as Figure 6, but for the semidiurnal phase  $t_{12}$ .

frequency, which is directly proportional to  $NmF2$ . However, the magnitude of the ratio,  $F_H/m_O\nu_{ni}$  changes little during daytime and decreases much at night, especially during early evening hours. Similar results can also be reached in other months. The model results show that the increase of the ion drag coefficients greatly compensates the pressure gradient force with increasing solar activity during night. It may largely explain the decreased diurnal amplitudes of the VEWs. It should be noted that we have not taken into account the solar activity dependence of ion velocity, which also influences the effect of ion drags.

[30] As seen in Figure 9, the diurnal component of  $F_H/m_O\nu_{ni}$  shifts later by  $\sim 9$  hours at solar maximum from solar minimum. Thus the relative increased control of ion drag may be the possible reason for the marked phase shift of VEWs for higher solar activity. If so, the solar activity and seasonal variation of the diurnal phase may have close relation with the ion/electron density, as suggested by Buonsanto [1991], and the different seasonal

variation of the diurnal phase between the southern and northern stations can be understandable based on the fact that the winter anomaly (maximum) of electron density appears mostly at northern midlatitude and especially at solar maximum, but it has few opportunities to occur at the Southern Hemisphere [Rishbeth, 1998]. However, much weaker phase delay is found in the diurnal component of  $F_H/m_O\nu_{ni}$  at Boulder in summer (not presented here). Reasons for this summer phase shift need further investigation.

#### 4.2. Solar Cycle Trends of the Diurnal Mean Winds

[31] Under quiet conditions at middle latitudes, the upward/downward equivalent winds correspond to equatorward/poleward meridional winds; therefore a positive correlation of the magnitude of the diurnal mean winds with  $F107$  implies less poleward or more equatorward neutral mean winds from solar minimum to solar maximum. Given that both the downward daytime equivalent winds and

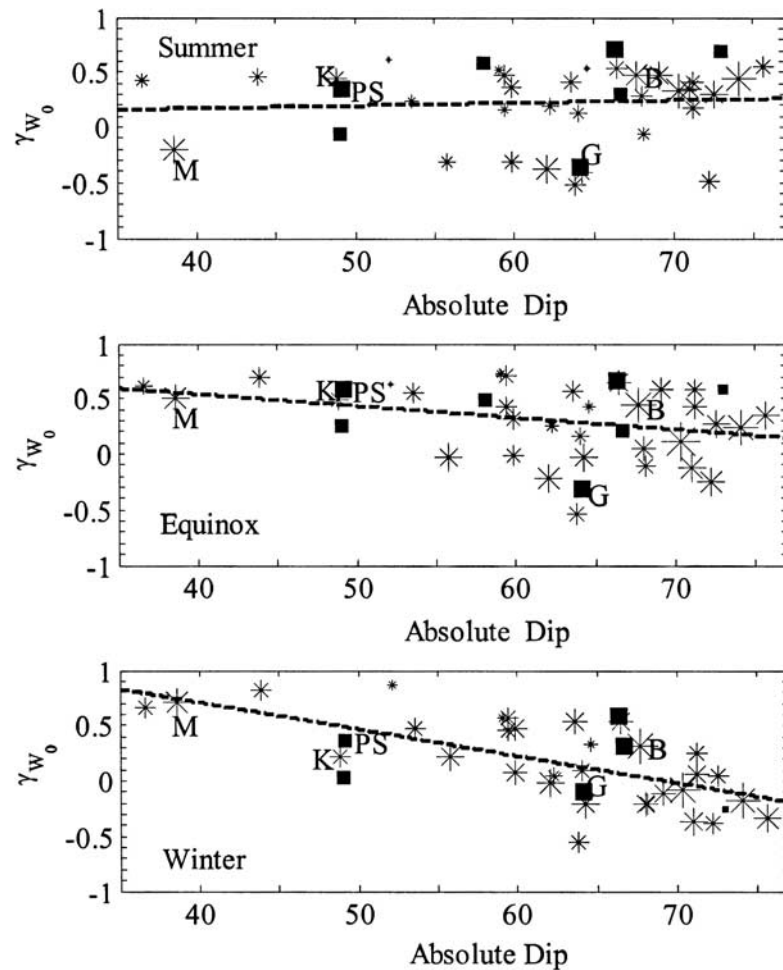


**Figure 8.** Same as Figure 6, but for the magnitude of the diurnal mean winds  $W_0$ .

upward nighttime ones tend to decrease with the increase of solar activity [Liu *et al.*, 2003c; Luan *et al.*, 2004], the prevailing positive solar activity trend may be explained by the fact that the largely downward VEWs are compensated more by the ion drag than the upward ones with increasing solar activity.

[32] The complicated solar activity variation of the diurnal mean VEWs may also attribute to their high variability at solar minimum. For example, the magnitude of the diurnal mean winds decrease uniformly from low to moderate solar activity in winter and equinox at Yamagawa. As a result, they have a strong correlation with  $F107$ . However, they decrease from downward/poleward flow to near zero at solar minimum and then decrease from considerable upward/equatorward to a smaller flow under moderate solar activity in summer at both Yamagawa and Tomsk, resulting in a considerable but not very strong correlation with  $F107$ . Also, in equinox and winter at Tomsk, the solar cycle variation for the mean winds is not clear under lower solar activity. The low peak height of the  $F2$  layer may introduce possible effects from the lower thermosphere, which may be one of the reasons of the highly scattered diurnal mean winds at solar minimum. Hedin *et al.* [1994] also reported that the diurnal mean winds from

the model prediction and various dataset differ most at solar minimum.

[33] There are also of different trends among ionosonde mean winds in previous studies. The ionosonde winds at Boulder and the ISR winds at Saint Santin show fairly weak trends of the diurnal mean winds with solar activity, while the Millstone Hill ISR winds show a shift from strong southward (equatorward) to near zero or northward (poleward) wind with increasing solar activity [Hedin *et al.*, 1994, and reference therein]. At King George Island, the mean equivalent winds are more poleward with increasing solar activity [Arriagada *et al.*, 1997], especially in winter; while at Kokubunji, the trends are just opposite [Igi *et al.*, 1999]. The contributions of  $\mathbf{E} \times \mathbf{B}$  drifts may be one of the factors inducing confusing solar activity trend of the diurnal mean. The contributions from the  $\mathbf{E} \times \mathbf{B}$  drifts are not extracted from the ionosonde winds at Kokubunji [Igi *et al.*, 1999] and at Wuhan [Liu *et al.*, 2003c] and in the present work.

#### 4.3. Effects of the Station Position

[34] The strong solar cycle trends of the diurnal component suggest a dominant control by the balance between the deriving force and the ion drag. However, this control seems much weaker for the semidiurnal compo-

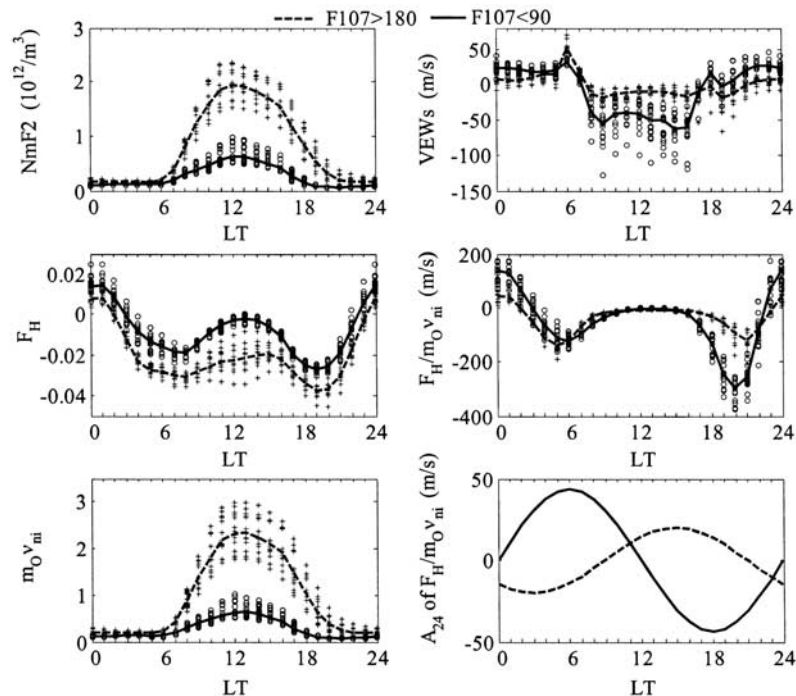


**Figure 9.** The monthly median (scattered points) and the corresponding median values (dashed and solid lines) of  $NmF2$  and VEWs and some related dynamic parameters at Boulder in December for  $F107 < 90$  and  $F107 > 180$ . The horizontal pressure gradient force  $F_H$ , the product of neutral-ion collision coefficient  $\nu_{ni}$  and the mass of atomic O  $m_O$ , the ratio  $F_H/m_O\nu_{ni}$ , and its diurnal component, respectively, which are evaluated from the IRI2000 and MSISE00 model with the observed median  $NmF2$  and  $hmF2$  as input parameters.

nents and the diurnal mean winds, at least at stations with higher latitudes. Our results for the solar cycle trends of the semidiurnal components and the diurnal mean winds depend on the dip angles (Figures 6–8). For the semidiurnal amplitude, our results are of general consistency at lower latitudes, where the semidiurnal amplitude has obviously significant correlation with solar activity than at higher latitudes except in winter. It may be associated with the important effect of the electric field drifts as well as the greater semidiurnal contribution to the neutral wind structure at lower latitudes [Hong and Lindzen, 1976; Luan *et al.*, 2004].

[35] Since the pressure gradients and neutral-ion drags are acted in the geographic meridian and along the magnetic field lines, respectively, the magnetic declination may modulate the solar cycle trends of the winds. The solar cycle trends of the diurnal components as a function of magnetic declination are shown in Figure 10. The solar cycle trend is weakest at Grahamstown, where declination is the largest among stations considered. In addition, different trends are also found at Maui. The unique feature in summer and weak trend in equinox at Maui may result from both the larger declination and the lowest geographical latitude among stations considered. It is interesting that the geographical latitude coincides with the geomagnetic latitude at the two stations, Grahamstown and Maui, which is unique among all stations.

[36] The bottom panel of Figure 10 also shows possible longitudinal effect on the solar cycle trends of the diurnal mean winds. The trends tend to be opposite at longitudinal

50–80°E and 90–160°E, where there is a relatively high convergence of ionosonde stations.

## 5. Summary

[37] A global climatology of winds at  $F$  region height is difficult to obtain because of lacking worldwide long-term data from incoherent scatter and Fabry-Perot measurements. Fortunately, equivalent winds can be derived from worldwide ionosonde measurements, which provide a valuable estimate for winds along the magnetic meridian. This investigation deals with the solar activity variations of the dominant tidal components of the equivalent winds at 39 stations in both hemispheres. Solar cycle variabilities of equivalent winds at so many stations for such long period are reported for the first time. The analysis of the equivalent winds shows the following.

[38] 1. The diurnal amplitude of the equivalent winds nonlinearly decreases with increasing solar activity at most stations and in all seasons, and its correlation with  $F107$  is strong, with absolute correlation coefficients higher than 0.7. This implies that the relative control from ion drag restrains the diurnal amplitude at high solar activity.

[39] 2. A general and evident feature found in the diurnal phase of the equivalent winds at most stations considered is that the diurnal phase tends to shift from local late evening to early morning with increasing solar activity. This is the first time to explicitly report the feature emerged at so many stations. Another pronounced feature is that the diurnal phase in the Northern Hemi-

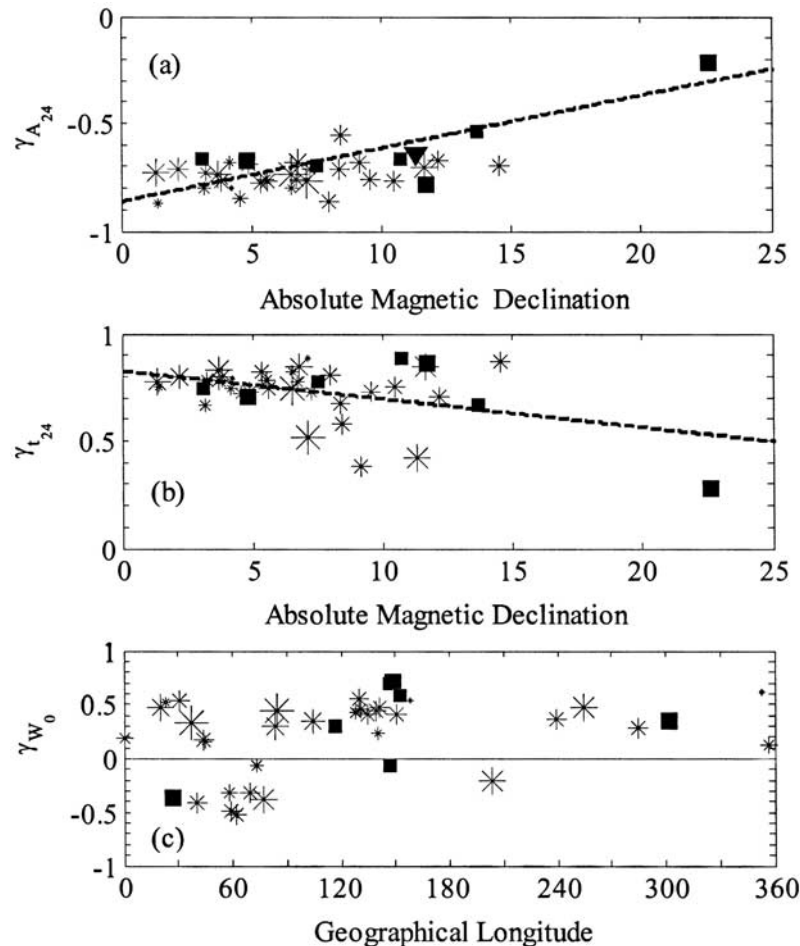


**Figure 10.** The control of geomagnetic declination on the solar cycle trends of the (a) diurnal amplitudes and (b) phases of the VEWs in summer and (c) the longitudinal dependence of the solar trends of the magnitude of diurnal mean winds in summer. The unique triangle in the top panel represents for  $-\gamma_{A_{24}}$  in summer at Maui.

sphere is generally later in winter than in summer for higher solar activity.

[40] 3. With increasing solar activity, a decrease in the semidiurnal amplitudes of equivalent winds is evident over most stations considered in summer. The decrease trend also is a general feature over a wide range of dip angle in winter and more significant at stations with a lower dip in other seasons. However, the diurnal mean and semidiurnal phase of the VEWs are of complicated solar activity dependences.

[41] **Acknowledgments.** Great appreciation to comments received from two reviewers, which lead to significant improvement of the quality of the manuscript. The ionosonde data used for this analysis are available in the American National Geophysical Data Center (NGDC-NOAA) database and the Japanese ionosonde data are provided from WDC for Ionosphere, Tokyo, National Institute of Information and Communications Technology. This research was supported by National Important Basic Research Project (G2000078407) and National Natural Science Foundation of China (40274054, 40134020).

[42] Arthur Richmond thanks Seiji Kawamura and Olivier G. Witasse for their assistance in evaluating this paper.

## References

Aruliah, A. L., A. D. Farmer, D. Rees, and U. Brandstrom (1996), The seasonal behavior of high-latitude thermospheric winds and ion velocities

observed over one solar cycle, *J. Geophys. Res.*, *101*(A7), 15,701–15,711.

Arriagada, M. A., A. J. Foppiano, and M. J. Buonsanto (1997), Solar activity variations of meridional winds over King George Island, Antarctica, *J. Atmos. Sol. Terr. Phys.*, *59*(12), 1405–1410.

Bilitza, D. (2001), International reference ionosphere 2000, *Radio Sci.*, *36*(2), 261–275.

Biondi, M. A., J. W. Meriwether, B. G. Fejer, S. A. Gonzalez, and D. C. Hallenbeck (1991), Equatorial thermospheric wind changes during the solar cycle: Measurements at Arequipa, Peru, from 1983 to 1990, *J. Geophys. Res.*, *96*, 15,917–15,930.

Biondi, M. A., S. Y. Sazykin, B. G. Fejer, J. W. Meriwether, and C. G. Fesen (1999), Equatorial and low latitude thermospheric winds: Measured quiet time variation with season and solar flux from 1980 to 1990, *J. Geophys. Res.*, *104*, 17,091–17,106.

Buonsanto, M. J. (1990), Observed and calculated F2 peak heights and derived meridional winds at mid-latitudes over a full solar cycle, *J. Atmos. Terr. Phys.*, *52*, 223–240.

Buonsanto, M. J. (1991), Neutral winds in the thermosphere at mid-latitude over a full solar cycle: A tidal decomposition, *J. Geophys. Res.*, *96*(A3), 3711–3724.

Buonsanto, M. J., and O. G. Witasse (1999), An updated climatology of thermospheric neutral winds and F region ion drifts above Millstone Hill, *J. Geophys. Res.*, *104*(A11), 24,675–24,687.

Duboin, M.-L., and M. Lefeuvre (1992), Thermospheric dynamics above Saint-Santin: Statistical study of the data set, *J. Geophys. Res.*, *97*(A6), 8661–8671.

Dudney, J. R. (1983), The accuracy of simple methods for determining the height of the maximum electron concentration of the F2-layer from scaled ionospheric characteristics, *J. Atmos. Terr. Phys.*, *45*(8/9), 629–640.

- Foppiano, A. J., X. A. Torres, M. A. Arriagada, and P. A. Flores (2003), Meridional thermospheric winds over the Antarctic Peninsula longitude sector, *J. Atmos. Sol. Terr. Phys.*, *65*, 305–314.
- Forbes, J. M., and H. B. Garrett (1978), Seasonal-latitude structure of the diurnal tide, *J. Atmos. Sci.*, *35*, 148–159.
- Hagan, M. E. (1993), Quiet time upper thermospheric winds over Millstone Hill between 1984 and 1990, *J. Geophys. Res.*, *98*(A3), 3731–3739.
- Hagan, M. E., and W. L. Oliver (1985), Solar cycle variability of exospheric temperature at Millstone Hill between 1970 and 1980, *J. Geophys. Res.*, *90*, 12,265–12,270.
- Hedin, A. E., M. J. Buonsanto, M. Codrescu, M.-L. Duboin, C. G. Fesen, M. E. Hagan, K. L. Miller, and D. P. Sipler (1994), Solar activity variations in midlatitude thermospheric meridional winds, *J. Geophys. Res.*, *99*(A9), 17,601–17,608.
- Hong, S.-S., and R. S. Lindzen (1976), Solar semidiurnal tide in the thermosphere, *J. Atmos. Sci.*, *33*, 135–153.
- Igi, S., W. L. Oliver, and T. Ogawa (1999), Solar cycle variations of the thermospheric meridional wind over Japan derived from measurements of hmF<sub>2</sub>, *J. Geophys. Res.*, *104*(A10), 22,427–22,431.
- Kawamura, S., Y. Otsuka, S.-R. Zhang, S. Fukao, and W. L. Oliver (2000), A climatology of middle and upper atmosphere radar observations of thermospheric winds, *J. Geophys. Res.*, *105*, 12,777–12,788.
- Liu, L., X. Luan, W. Wan, J. Lei, and B. Ning (2003a), Seasonal behavior of equivalent winds over Wuhan derived from ionospheric data in 2000–2001, *Adv. Space. Res.*, *32*, 1765–1770.
- Liu, L., X. Luan, W. Wan, B. Ning, and J. Lei (2003b), A new approach to the derivation of dynamic information from ionosonde measurements, *Ann. Geophys.*, *21*(11), 2185–2191.
- Liu, L., W. Wan, X. Luan, B. Ning, and J. Lei (2003c), Solar activity dependence of the effective winds derived from ionospheric data at Wuhan, *Adv. Space. Res.*, *32*, 1719–1724.
- Luan, X., L. Liu, J. Lei, W. Wan, and B. Ning (2002), Deriving equivalent winds from ionospheric F-layer data (in Chinese), *Chin. J. Space Sci.*, *22*(2), 119–128.
- Luan, X., L. Liu, W. Wan, J. Lei, and T. Yu (2004), Climatology of the F-layer equivalent winds derived from ionosonde measurements over two decades along the 120°–150E° sector, *Ann. Geophys.*, *22*(8), 2785–2796.
- Miller, K. L., D. G. Torr, and P. G. Richards (1986), Meridional winds in the thermosphere derived from measurements of F<sub>2</sub> layer height, *J. Geophys. Res.*, *91*(A6), 4531–4535.
- Miller, K. L., J. E. Salah, and D. G. Torr (1987), The effect of electric fields on measurements of meridional neutral winds in the thermosphere, *Ann. Geophys.*, *5A*(6), 337–342.
- Picone, J. M., A. E. Hedin, D. P. Drob, and A. C. Aikin (2002), NRLMSISE-00 empirical model of the atmosphere: Statistical comparisons and scientific issues, *J. Geophys. Res.*, *107*(A12), 1468, doi:10.1029/2002JA009430.
- Richards, P. G. (2001), Seasonal and solar cycle variations of the ionospheric peak electron density: Comparison of measurement and models, *J. Geophys. Res.*, *106*(A7), 12,803–12,819.
- Rishbeth, H. (1998), How the thermospheric circulation affects the ionospheric F<sub>2</sub>-layer, *J. Atmos. Sol. Terr. Phys.*, *60*, 1385–1402.
- Titheridge, J. E. (1995), Winds in the ionosphere—A review, *J. Atmos. Terr. Phys.*, *57*(14), 1681–1714.
- Witasse, O., J. Lilensten, C. Lathuillere, and B. Pibaret (1998), Meridional thermospheric neutral wind at high latitude over a full solar cycle, *Ann. Geophys.*, *16*, 1400–1409.

J. Lei and X. Luan, Wuhan Institute of Physics and Mathematics, Chinese Academy of Sciences, Wuhan 430071, China.

L. Liu, B. Ning, and W. Wan, Institute of Geology and Geophysics, Chinese Academy of Sciences, Beijing 100029, China. (liul@mail.iggcas.ac.cn; nbq@mail.iggcas.ac.cn; wanw@mail.iggcas.ac.cn)